Zoom-in X-ray Micro Tomography System

In Kon Chun, Sang Chul Lee, Jeong Jin Park, Min Hyoung Cho, Soo Yeol Lee

Functional and Metabolic Imaging Research Center
Department of Biomedical Engineering, Kyung Hee University, Korea

Abstract: We introduce an x-ray micro tomography system capable of high resolution imaging of a local region inside a small animal. By combining two kinds of projection data, one from a full field-of-view (FOV) scan of the whole body and the other from a limited FOV scan of the region of interest, we have obtained zoomed-in images of the region of interest without any contrast anomalies. We have integrated a micro tomography system using a micro-focus x-ray source, a 1248×1248 flat-panel x-ray detector, and a precision scan mechanism. Using the cross-sectional images taken with the zoom-in micro tomography system, we measured trabecular thicknesses of femur bones in postmortem rats. To compensate the limited spatial resolution in the zoom-in micro tomography images, we used the fuzzy distance transform for the calculation of the trabecular thickness. To validate the trabecular thickness measurement with the zoom-in micro tomography images, we compared the measurement results with the ones obtained from the conventional micro tomography images of the extracted bone samples.

Key words: Zoom-in micro tomography, Flat panel detector, Fuzzy distance transform, Trabecular thickness, Osteoporosis

INTRODUCTION

Recently, small-animal imaging technology has been rapidly developed for longitudinal screening of laboratory animals raised with disease developments or genetic manipulations [1-3]. It is of paramount importance in the biomedical field to screen laboratory animals in a minimally invasive way since longitudinal studies through the lifetime of the small animals are essential in the investigation of new drug/therapy effect with human disease models [4, 5]. Among the newly developed small animal imaging modalities, x-ray micro tomography, often called x-ray micro-CT, is believed to be very potential for anatomical imaging in a minimally invasive way [6-8]. Most of micro-CTs are capable of μm-resolution imaging when they are applied to small sample imaging. However, the spatial resolution of micro-CTs in the small animal imaging should be sacrificed down to the order of 100 μm due to the limited number of x-ray detector pixels and low signal-to-noise ratio.

Corresponding Author : Soo Yeol Lee, Professor
Department of Biomedical Engineering Kyung Hee University
1 Seochun, Kiheung, Yongin, Kyungki 449-701 South Korea
Tel. +82-31-201-2980   Fax. +82-31-201-3666
E-mail. sylee01@khu.ac.kr

In this study, we introduce an x-ray micro tomography system which has zoom-in imaging capability, i.e., high resolution imaging of a local region of interest (ROI) inside a large object, in small animal studies. We have integrated a micro tomography system using a micro-focus x-ray source, a 1248×1248 flat-panel x-ray detector, and a precision scan mechanism. To verify the utility of the zoom-in micro tomography system, we have measured trabecular thickness in the femurs of postmortem SD rats with the zoom-in micro tomography technique without extracting the femurs from the rats. To evaluate accuracy of the trabecular thickness measurements with the zoom-in micro tomography of whole rats, we have also measured trabecular thicknesses in the femurs extracted from the same rats.

THE ZOOM-IN MICRO TOMOGRAPHY SYSTEM

Principles of Zoom-in Micro Tomography

In zoom-in micro tomography, two projection data sets, one obtained with a full FOV scan and the other obtained with a limited FOV scan, are acquired with different magnification ratios. We denote the two

projection data sets as $P_1(\alpha, x')$ and $P_2(\alpha, x')$ as shown in Fig. 1 (a) and (b). □ is the rotation angle of the fan-beam about the rotation center O_1 or O_2, respectively, and x' is the horizontal distance between the given ray and the center point D on the detector plane. Since we use a flat-panel detector for the acquisition of the projection data, we will consider the equi-space fan-beam mode scan rather than the equi-angle fan-beam mode scan. In a conventional micro tomography system, the x-ray source and the x-ray detector are fixed at the given positions and the sample holder is rotated at a constant angular speed for the scan. The sample holder is mounted on a precision translator to control the magnification ratio of the imaging. The magnification ratio is determined by SD/SO where SD and SO are the source-to-detector distance and the source-to-object distance, respectively.

Since the limited FOV projection data, $P_2(\alpha, x')$, are incomplete, i.e., the projection data are missing outside the FOV, we cannot reconstruct exact images of the ROI using $P_2(\alpha, x')$. To obtain exact images of the ROI, we reconstruct the complete projection data $P_2'(\alpha, x')$ by combining the two projection data, $P_2'(\alpha, x') = P_2(\alpha, x')$ when $-x_m \leq x' \leq x_m$, and $P_2'(\alpha, x') = P_2^r(\alpha, x')$ when $|x'| \geq x_m$, in which x_m is half the horizontal width of the detector plane and $P_2'(\alpha, x')$ is the projection data outside the FOV calculated from the full FOV image. For the calculation of $P_2'(\alpha, x')$, we first reconstruct a full FOV image from the full FOV projection data $P_1(\alpha, x')$ using the equi-space fan-beam image reconstruction algorithm [9], and then, we calculate $P_2^r(\alpha, x')$ with ray tracing through the reconstructed full FOV image [10] as shown in Fig. 1(c). Once the projection data calculation is completed, the two projection data, one measured and the other calculated, are combined as shown in Fig. 1(d) for the reconstruction of ROI images.

Integration of a Zoom-in Micro Tomography System

A schematic diagram of the integrated micro tomography system is shown in Fig. 2. The micro tomography system consists of a micro-focus x-ray source, a rotating object holder, a CMOS flat-panel detector, and a parallel data processing system. All the components except the data processing system are mounted on an optical bench. The source-to-object distance SO and source-to-detector distance SD can be varied to control the imaging parameters such as magnification ratio and FOV. In this study, SD was set to 509mm, and SO was varied with a computer-controlled translation system with an accuracy of 10 μm. A computer-controlled rotation system was also adopted in the object holder to achieve a cone-beam mode scan in the micro tomography system. The precision of the rotational motion is 0.083°.

The micro-focus x-ray source (Ultra Bright, Oxford Instruments, UK) is a sealed tube with a fixed tungsten anode having an angle of 15° against the electron beam and with a 245-μm-thick beryllium exit window. The emitted x-ray beam angle is about 33°. The source has a variable focal spot size from 12 μm to 40 μm depending on the applied tube power (Watt or kVp × mA). The maximum tube voltage and tube current are 90 kVp and 2 mA, respectively. The micro-focus x-ray source has been operated in a continuous mode with an Al filter with the thickness of 1mm.

A 2D flat-panel detector (C7943CP-02, Hamamatsu, Japan) has been used for the projection data acquisition in the micro-CT system. The flat-panel detector consists of a 1248 × 1248 active matrix of transistors and photodiodes with a pixel pitch of 100
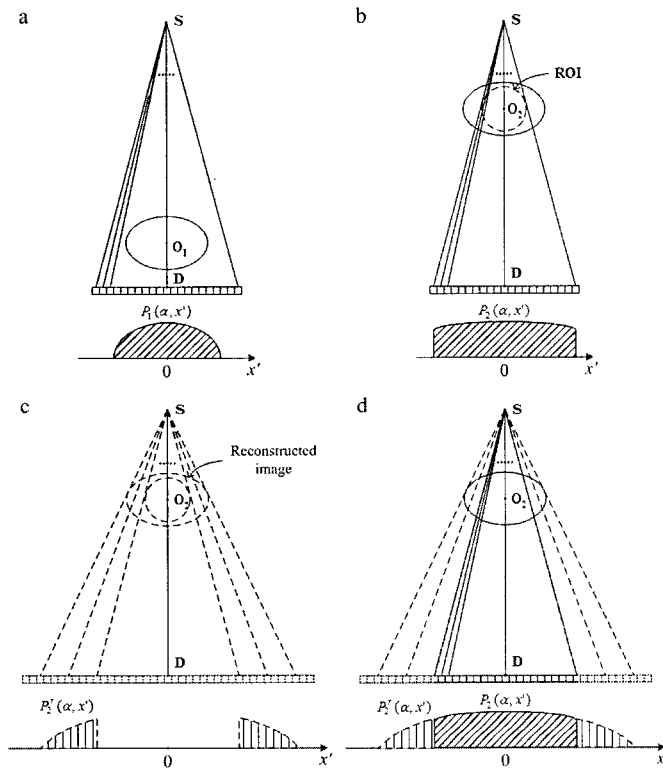

Fig. 1. Schematic diagrams of the projection data acquisition in zoom-in micro tomography. S and D are the x-ray source target point and the center of the detector plane, respectively, and O_l is the rotation axis of the fan-beam scan. (a) Acquisition of the full FOV projection data $P_1(\alpha, x')$. (b) Acquisition of the limited FOV projection data $P_2(\alpha, x')$. (c) Calculation of the projection data from the full FOV image outside the limited FOV. (d) Combination of the limited FOV projection data $P_2(\alpha, x')$ (the solid lines) with the calculated projection data outside the limited FOV (the dashed lines).

μm, and a CsI:Tl scintillator. The detector was fabricated with the CMOS process capable of a submicron line width resolution [11]. The pixel fill factor is 80%, in spite of the small pixel size of 100 μm.

To realize a parallel data processing system for image reconstruction, we have linked four personal computers, each one equipped with dual CPUs (Athlon MP 2200+, AMD, USA), with 100 Mbps Ethernet and assigned evenly divided tasks to each of the eight CPUs. One of the four computers was chosen as a host computer and the host computer controlled the whole micro-CT system.
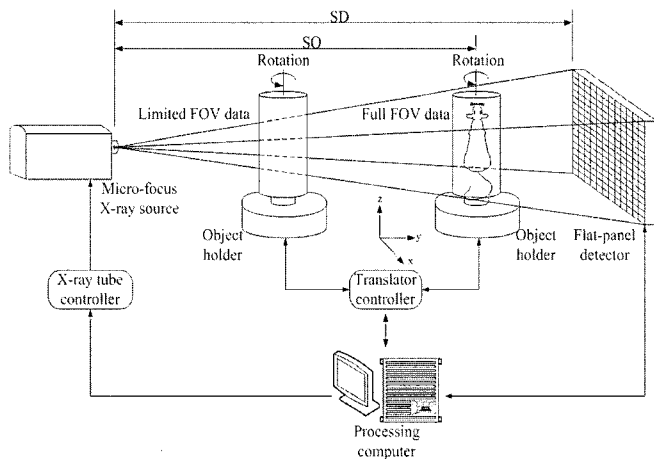

Fig. 2. A schematic diagram of the zoom-in micro tomography system.

EXPERIMENTAL RESULS

Performance Evaluations of the Zoom-in Micro Tomography System

To experimentally validate the proposed technique, we evaluated the spatial resolution and contrast-to-noise performance of the developed micro-CT system. In the spatial resolution measurements, we took cross-sectional images of a thin gold wire with the diameter of 20 □m. We set SD and SO to 509mm and 422mm, respectively, in the full FOV imaging, and we changed SO to 103mm in the zoom-in imaging. Hence, the magnification ratios were 1.2 and 4.9 in the full FOV imaging and the zoom-in imaging, respectively. After obtaining the cross-sectional gold wire image $g(x,y)$, we calculated one-dimensional Fourier transform, $G(k_x)$, of the center profile of the gold wire image, i.e., $g(x,0)$. To take into account the non-zero width of the gold wire, we divided $G(k_x)$ by the Fourier transform of the profile function of the gold wire. The dividend, then, represents the modulation transfer function (MTF) of the micro-CT. For the gold wire imaging, we applied the

tube voltage and current of 60kV and 1.3mA, respectively. The number of views was 900 over 360 degrees and the frame time was 250ms. Figure 3 shows the MTF measurement results. The MTFs of the full FOV imaging and the zoom-in imaging are shown as circles and squares, respectively. If we assume that the limiting spatial resolution corresponds to the point when the MTF drops to 10%, we can infer that the spatial resolution limits of the micro-CT system are about 10 lp/mm and 4 lp/mm in the zoom-in imaging and the full FOV imaging, respectively. The spatial resolution improvement in zoom-in imaging is about 2.5. Since the magnification ratio of the zoom-in imaging is about 4 times bigger than the full FOV imaging, the limit in the spatial resolution improvement of the zoom-in imaging will be about 4. The rather small improvement in the spatial resolution is thought to be caused by the finite focal spot size and the scattering effect in the phantom.
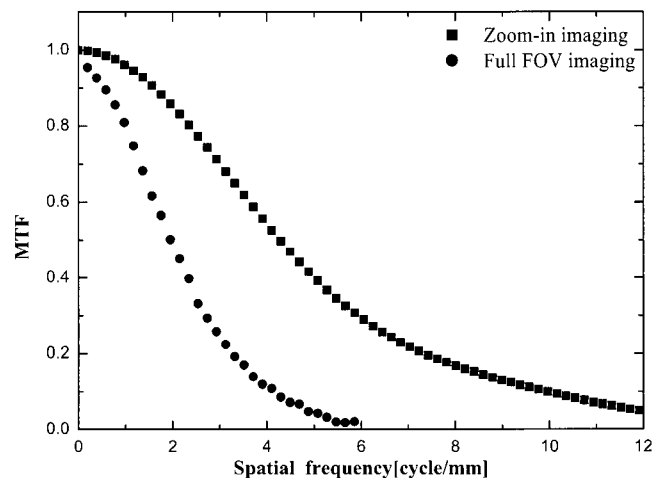

Fig. 3. Measured MTFs of the zoom-in micro tomography system. The magnification ratios are 1.2 and 4.9 in the full field-of-view imaging and the zoom-in imaging, respectively.

We have tested low-contrast visibility of zoom-in imaging using a contrast phantom shown in Fig. 4(a). SD and SO were set to the same as the MTF measurements. The contrast phantom consists of six inserts whose physical densities are similar to that of water. The six inserts with 5 mm diameter were immersed in a water bath made of a 40 mm diameter acryl cylinder. The inserts were made of commercial electron density phantoms (Model 76-430, Nuclear Associates, NY, USA). Physical properties of the six inserts are shown in Table 1. For the contrast phantom imaging, we applied the tube voltage and current of 45kV and 1.8mA, respectively. The number of views was 900 over 360 degrees and the frame time was 555 ms with the scan time of 9 min. Figure 4(a) and (b)

shows the cross-sectional images of the contrast phantom obtained with the full FOV imaging and the zoom-in imaging, respectively. The detector slice thicknesses in the full FOV imaging and the zoom-in imaging are 100μm and 300μm, respectively, which correspond to 83μm and 60μm in actual slice thickness. The insert A is not discriminated in both images. The pixel mean values and standard deviations at the six insert regions are shown in Table 1. As can be noticed from Table 1, the contrast values in the zoomed-in image are very similar to the ones in the full FOV image. The noises, i.e., standard deviations, in the zoomed-in images are about 2.5~3 times bigger than they are in the full FOV image. Since SNR of a CT image is inversely proportional to $\Delta x \sqrt{H}$ (μx: pixel size, H: detector slice thickness) if the system noise is neglected [12], the degree of SNR degradation of the zoomed-in images could be as big as 2.4 times. The little bit more SNR degradation is due to the stronger ring artifacts in the zoom-in imaging.

Table 1. Mean pixel values and standard deviations in the contrast phantom image.

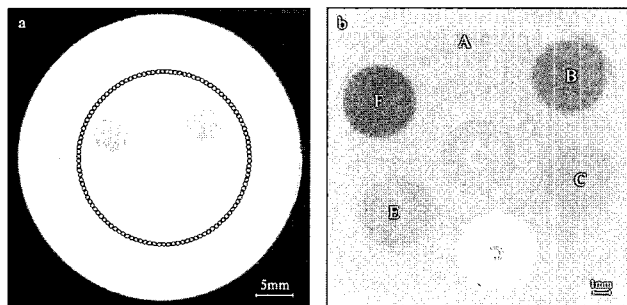| Regions (Material, density[g/cm³])	Mean pixel values± standard deviations	
	Full FOV imaging	Zoom-in imaging
A(Acrylic, 1.180)	5.09±0.22	5.19±0.61
B(Polystyrene, 1.110)	4.13±0.24	4.12±0.61
C(Polycarbonate, 1.180)	5.03±0.25	4.97±0.64
D(Plastic water, 1.030)	8.03±0.24	8.20±0.69
E(Nylon, 1.150)	4.97±0.21	4.99±0.62
F(Polyethylene, 0.950)	3.94±0.24	3.94±0.62

Fig. 4. (a) The full field-of-view image of the contrast phantom. (b) The ROI image of the contrast phantom taken with the zoom-in micro tomography system.

Trabecular Bone Thickness Measurement

After positioning the femur region at the middle of the scan volume, we obtained zoom-in micro tomography images of three postmortem SD rats. Each rat weighed about 300g. Figure 5(a), (b) and (c) show three representative consecutive zoom-in micro tomography images of the femur region of one of the SD rats. The slice thickness and slice gap are 69μm and 207μm, respectively. In the zoom-in micro tomography scan, we applied the tube voltage and current of 50kV and 0.20mA for the limited FOV scan and 50kV and 0.5mA for the full FOV scan, respectively.
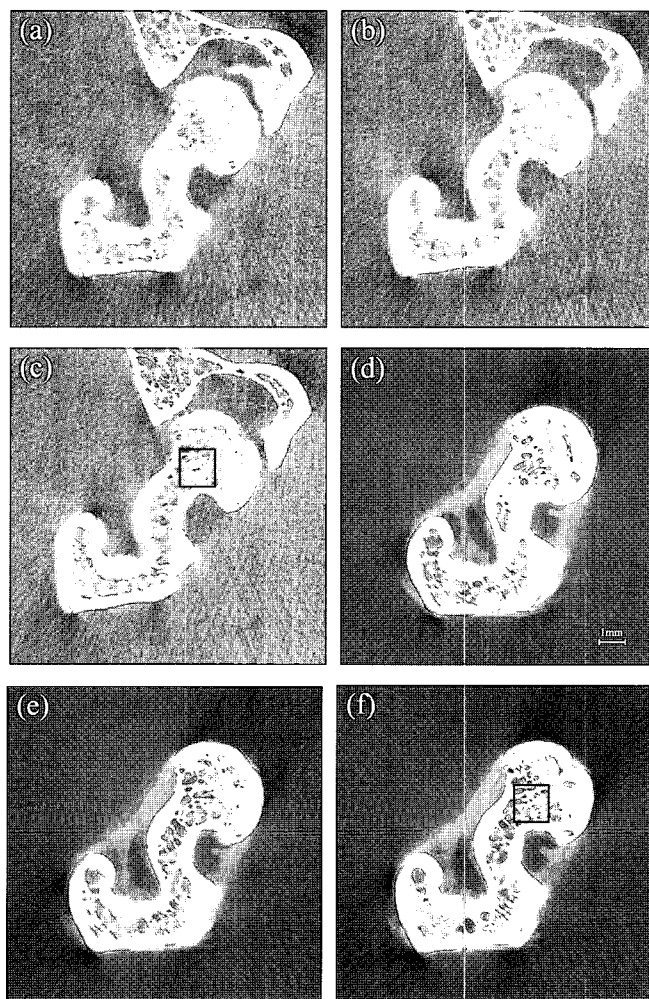

Fig. 5. (a)(b)(c) Five consecutive zoom-in micro tomography images of the femur region in a SD rat (slice thickness = 69μm, slice gap=138μm). (d)(e)(f) Corresponding conventional micro tomography images of the femur sample extracted from the rat (slice thickness = 23μm, slice gap=184μm).

The numbers of views were 600 and 180 in the limited FOV scan and in the full FOV scan, respectively. To reduce the total scan time, the detector frame time was set to 0.5 s in the full FOV scan while it was set to 2 s in the limited FOV scan to compromise the low signal-to-noise ratio. The pixel size of the zoom-in micro tomography images is about 23μm with the magnification ratio of 4.4. Owing to the improved spatial resolution of the zoom-in micro tomography as compared with the conventional micro tomography, we can observe the trabecular component in the femur much more clearly. To compare the zoom-in micro tomography images of the femur region with the conventional micro tomography images, we extracted the femurs from the rats after the zoom-in micro tomography scan. The extracted femurs were, then, imaged with the conventional micro tomography technique with the same magnification ratio of 4.4 and the slice thickness of 23μm. The femur sample image was taken with isotropic voxel size of 23μm³ to obtain high spatial resolution reference images. Three consecutive images of the extracted femur corresponding to Fig. 5(a), (b) and (c) are shown in Fig. 5(d), (e), and (f), respectively. The conventional micro tomography images are a little different from the corresponding zoom-in tomography images due to different orientation of the femur in the two types of the tomography scan.

We used the fuzzy distance transform (FDT) to calculate the mean trabecular bone thickness at the regions of interest in the femur images [13, 14], and the results are summarized in Table 2. As can be noticed from Table 2, the mean trabecular thicknesses calculated from the zoom-in micro tomography images are quite similar to those calculated from the conventional micro tomography images of the extracted femurs, demonstrating the utility of the zoom-in micro tomography in bone studies. The average difference between the two types of measurement results is less than 2.5%. To further validate the trabecular thickness measurements with the zoom-in micro tomography technique, we have compared the trabecular thickness histograms obtained from the two kinds of tomographic images.

Figure 6 shows the trabecular thickness histograms of the three rats. Figure 6(a) and (b) represent the results obtained from the zoom-in micro tomography images of the femur regions and the conventional micro tomography images of the extracted femurs, respectively.
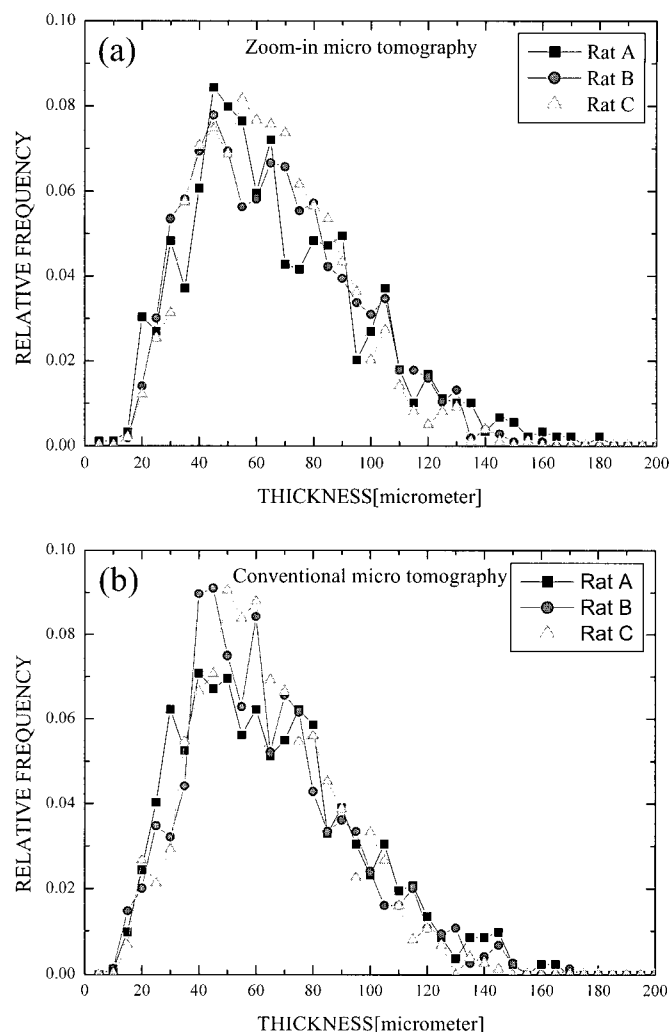

Fig. 6. Trabecular thickness histograms calculated from (a) the zoom-in micro tomography images of the femur regions of three SD rats and (b) the conventional micro tomography images of the femur samples extracted from the rats.

Table 2. Trabecular thickness measurement results (μm)

Subjects	Measured with zoom-in tomography images of the femur region	Measured with conventional micro tomography images of the extracted femur samples
Rat A	70.7	69.7
Rat B	62.9	62.9
Rat C	65.7	64.1

DISCUSSIONS AND CONCLUSIONS

The major drawbacks of zoom-in micro tomography are two times longer scan time and more x-ray exposure. The latter may limit the longitudinal small animal studies more severely since current micro tomography technology still have limitations in

longitudinal small animal studies due to its excessive x-ray exposure to overcome low signal-to-noise ratio. In small animal imaging with a micro-CT, long scan time to secure sufficient soft tissue contrast is often troublesome. In small animal imaging with the flat panel detector based micro-CT, a scan time of at least several minutes is inevitable to differentiate soft tissues. Even with a highly sensitive x-ray detector such as a CCD coupled with an optical taper, it seems that long scan time is unavoidable in small animal imaging. Due to the long scan time, rat or mouse imaging *in vivo* suffers from cardiac and respiratory motion artifacts. Motion artifacts in zoom-in micro tomography should be investigated in the future imaging studies of live small animals.

Although the trabecular thickness measurements have been performed on postmortem rats, we think the experimental results demonstrate the utility of the zoom-in micro tomography technique in bone studies with laboratory small animals. Further developments are still necessary to apply the zoom-in micro-tomography technique to bone studies *in vivo*. First of all, we need to devise techniques to reduce motion artifacts. Despite the motion artifacts, however, our preliminary *in vivo* imaging studies of SD rats suggest that bone studies with live small animals are possible with zoom-in micro tomography if the small animal subject is tightly fixed not to have excessive motions. We are now developing a gantry rotating zoom-in micro tomography system to reduce the motion artifacts.

In conclusions, a zoom-in micro tomography system has been developed with a flat-panel x-ray detector and a micro-focus x-ray source. The zoom-in micro tomography technique has been used in trabecular thickness measurement in bone studies with small animals without extracting the bone of interest. We expect that longitudinal studies with live small animals are possible in the near future.

REFERENCES

[1] T. F. Massoud and S. S. Gambhir, *"Molecular imaging in living subject: seeing fundamental biological processes in a new light"*, Genes & Development, Vol. 17, pp. 545-580, 2003.

[2] M. G. Pomper, *"Molecular imaging: an overview"*, Acad. Radiol., Vol. 8, pp. 1141-1153, 2001.

[3] R. Weissleder and U. Mahmood, *"Molecular imaging"*, Radiology, Vol. 219, pp. 316-333, 2001.

[4] M. J. Paulus, S. S. Gleason, H. Sari-Sarraf, D. K. Johnson, C. J. Foltz , D. W. Austin, M. E. Easterly, E. J. Michaud, M. S. Dhar, P. R. Hunsicker, J. W. Wall and M. Schell, *"High-resolution x-ray CT screening of mutant mouse models"*, Proc. SPIE, Vol. 3921, pp. 270-279, 2000.

[5] E. L. Ritman, *"Molecular imaging in small animals-roles for micro-CT"*, J. Cell. Biochem., Supp. 39, pp. 116-124, 2002.

[6] S. M. Jorgensen, O. Demirkaya and E. L. Ritman, *"Three-dimensional imaging of vasculature and parenchyma in intact rodent organs with x-ray micro-CT"*, Am. J. Physiol., Vol. 275, H. 1103-1114, 1998.

[7] M. J. Paulus, H. Sari-Sarraf, S. S. Gleason, M. Bobrek, J. S. Hicks, D. K. Johnson, J. K. Behel, L. H. Thompson and W. C. Allen, *"A new x-ray computed tomography system for laboratory mouse imaging"*, IEEE. Trans. Nucl. Sci., Vol. 46, pp. 558-564, 1999.

[8] S. Y. Wan, A. P. Kiraly, E. L. Ritman and W. E. Higgins, *"Extraction of the hepatic vasculature in rats using 3-D micro-CT images"*, IEEE. Trans. Med. Imag., Vol. 19 pp. 964-971, 2000.

[9] A. C. Kak and M. Slaney, Algorithms for reconstruction with nondifferacting sources, In: Principles of computed tomography imaging, New York: IEEE Press, pp. 86-92, 1988.

[10] Z. H. Cho, Image reconstruction from projection in two dimensions, In: Foundations of medical imaging, Singaporer: John Wiley & Sons, Inc., pp. 71-81, 1983.

[11] H. Mori, R. Kyuushima, K. Fujita and M. Honda, *"High resolution and high sensitivity CMOS panel sensors for x-ray"*, IEEE Nucl. Sci. Sym. & Med. Imag. Conf. Conference Record in CD-ROM, 2001.

[12] D. W. Holdsworth, M. Drangova and A. Fenster, *"A high-resolution XRII-based quantitative volume CT scanner"*, Med. Phys., Vol. 20 pp. 449-462, 1993.

[13] P. K. Saha, F. W. Wehrli and B. R. Gomberg, *"Fuzzy distance transform: theory, algorithms, and applications"*, Comput. Vis. Image Und., Vol. 86 pp. 171-90, 2002.

[14] P. K. Saha and F. W. Wehrli, *"Measurement of trabecular bone thickness in the limited resolution region of in vivo MRI by fuzzy distance transform"*, IEEE Trans. Med. Imag., Vol. 23 pp. 53-62, 2004.